

Preparation and characterization of scutellarin loaded on ultradeformable nano-liposomes scutellarin EDTMP (S-UNL-E) and in vitro study of its osteogenesis

Teng Minhua^{a,b}, Wang Dashan^{a,b}, Shi Xinyan^c, Yuan Xiao^{b,d}, Li Xiaojing^{a,b}, and Zhao Baodong^{a,b}

^aDepartment of Oral Implantology, The Affiliated Hospital of Qingdao University, Qingdao, China; ^bSchool of Stomatology, Qingdao University, Qingdao, China; ^cParty and Administration Office, the Affiliated Hospital of Qingdao University, Qingdao, China; ^dDepartment of Orthodontics, The Affiliated Hospital of Qingdao University, Qingdao, China

ABSTRACT

The present research aimed to elucidate a convenient, safe and economic approach to induce the growth of endogenous bone tissue and bone regeneration. S-UNL-E was prepared using reverse-phase evaporation, and scutellarin encapsulation was subsequently compared. Meanwhile, the optimal preparation scheme was developed using an orthogonal method, and the particle size was determined using laser light scattering. In osteoblasts cultured in vitro, methyl thiazolyl tetrazolium (MTT), alkaline phosphatase (ALP) staining and alizarin red staining were used to detect the osteogenic effects of S-UNL-E. The results indicated that the optimal process conditions for S-UNL-E included mass ratios of phospholipid-cholesterol, phospholipid-brevicapsin, phospholipid-sodium cholate, and phospholipid-stearamide were 2:1, 15:1, 7:1 and 7:1, respectively, and the mass of ethylenediamine tetramethylphosphonic acid (EDTMP) was 30 mg. The average particle size of S-UNL-E was 156.67 ± 1.76 nm, and Zeta potential was -28.77 ± 0.66 mv. S-UNL-E substantially increased the expression of ALP osteoblasts, elevated the content of osteocalcin protein and promoted the formation of mineralized nodules. Cells in the S-UNL-E group were densely distributed with integrated cell structure, and the actin filaments were clear and obvious. The findings demonstrated that S-UNL-E greatly promoted the differentiation and maturation of osteoblasts, and S-UNL-E (2.5×10^8) produced the most favorable effect in differentiation promotion. In conclusion, the present study successfully constructed an S-UNL-E material characterized by high encapsulation and high stability, which could effectively promote osteogenic differentiation and bone formation.

ARTICLE HISTORY

Received 25 October 2021
Revised 3 December 2021
Accepted 4 December 2021

KEYWORDS





S-UNL-E; scutellarin;
osteogenic differentiation;
encapsulation

1. Introduction

Implant dentures have emerged as the first choice of patients with tooth loss for denture restoration and are known as the ‘third pair of teeth’. However, a variety of factors have caused poor bone mass and bone quality in the implantation area, which is a challenge in successful implant restoration [1,2]. Scutellarin (SCU), a novel flavonoid agent, is a major effective component of the Chinese herb *Scutellaria baicalensis Georgi*. SCU functions in dilating microvessels, reducing blood viscosity, increasing cerebral blood flow and improving microcirculation and lipid metabolism. It also assists in anti-inflammation, anti-apoptosis, anti-oxidation and anti-allergic [3–6]. A recent study has confirmed that SCU can regulate bone metabolism. It upregulates the transcriptional activity and mRNA

expression level of bone morphogenetic protein 2 (BMP2) and induces osteogenic differentiation by activating the BMP pathway. Meanwhile, it inhibits osteoclastogenesis and prevents Ti particle-induced osteolysis by suppressing RANKL-mediated mitogen-activated protein kinase (MAPK) and NF- κ B signaling pathway [7,8].

Due to the biological particularity of bone tissues, such as high hardness, poor permeability and low blood flow, it is difficult to use drugs in clinic [9]. According to traditional methods of drug delivery, drugs are rarely transported to the exact bone lesions. Moreover, low curative effect and large adverse reactions are common shortcomings of systemic administration in the treatment of bone-related diseases. In recent decades,

CONTACT Teng Minhua  dentisteng@qdu.edu.cn  The Affiliated Hospital of Qingdao University, Qingdao 266000, China; Zhao Baodong  zbd315@sina.com
 The Affiliated Hospital of Qingdao University, Qingdao China

© 2022 The Author(s). Published by Informa UK Limited, trading as Taylor & Francis Group.
This is an Open Access article distributed under the terms of the Creative Commons Attribution-NonCommercial License (<http://creativecommons.org/licenses/by-nc/4.0/>), which permits unrestricted non-commercial use, distribution, and reproduction in any medium, provided the original work is properly cited.

nanotechnology has gained increasing attention in the medicine field because of its remarkable nano-size effect, which has shown superiority over traditional formulations for local topical therapy [10].

A good drug sustained-release system can reduce the possible side effects of drugs, achieve drug release and targeting, and avoid premature diffusion and clearance of drugs. Presently, liposome has attracted much attention because of its simple preparation, nontoxic, and non-immunogenic. This therapy is easy to be implemented and available for release of multiple drugs as well as feasible to be modified to reach specific sites [11]. In addition, molecular docking and photoelectrochemical biosensing have been widely studied and designed to test targets and sensitivity [12,13]. The concept of 'bone targeting' means that compound molecules have the tendency to deposit in bone and incorporate hydroxyapatite, which can also bind to bone calcium [14–16]. Therefore, any molecule with specific affinity to hydroxyapatite can be used as the guide or carrier of bone targeting drugs, so that the drugs can selectively act on bone tissue. Polyphosphate compounds have high affinity to bone, especially bone matrix. The representative compound EDTMP has been widely studied and applied as a bone target carrier of radionuclides [17,18].

We speculated that S-NUL-E could promote bone formation and improve bone mass and bone quality in the implantation area. The purpose of this study was to screen the optimal process conditions and concentration of S-NUL-E and to construct S-UNL-E with high encapsulation and high stability. This study developed S-NUL-E and the optimum formula was obtained through experiments. The physicochemical properties of S-NUL-E were characterized, and their bio-activity was evaluated *in vitro*. Our results demonstrated the potential of S-NUL-E in treating poor bone mass and bone quality in the implantation area by its osteogenesis.

2. Materials and methods

Scutellarin (CAS:27740–01-8) was sourced from MedChemExpress (New Jersey, the United States), soy lecithin (CAS:8002–43-5) from Tokyo Chemical Industry (Tokyo, Japan), sodium cholate

(CAS:361–09-1) from Macklin (Shanghai, China), stearamide (CAS:124–26-5) from Macklin (Shanghai, China), cholesterol from Fuyu Fine Chemical Co. LTD. (Tianjin, China) and phosphate-buffered solution from Punosai Life Technology Co. LTD. methyl alcohol and acetonitrile (high-pressure liquid chromatography grade) were obtained from Fuyu Fine Chemical Co. LTD (Wuhan, China). All reagents were of analytical grade and used without further purification.

2.1 Preparation of S-UNL-E

S-NUL-E were prepared by a reverse phase evaporation method [19]. Briefly, soy lecithin, sodium cholate, sodium cholate, cholesterol and EDTMP were dissolved in chloroform (containing 1% anhydrous ethanol). Phosphate-buffered solution containing scutellarin was added to a lipid film. The obtained suspensions were sonicated in a water bath ultrasonic instrument for 10 min (intermittent operation for 10 s on and 5 s off), then the solvent was removed under reduced pressure by a rotary evaporator. The suspension was transferred to a syringe, filtered with a polyamide filter membrane and sealed for storage using nitrogen.

2.2 Determination of encapsulation efficiency of S-UNL-E

Dextran gel (g-50) was dissolved in PBS at room temperature. Swollen g-50 and S-UNL-E were added to the syringe. To separate liposomes and drugs, liposomes were removed via centrifugation (3000 rpm, 4°C and 3 min). Thereafter, the supernatant was collected and diluted. The encapsulation efficiency of S-UNL-E was calculated using HPLC. Liposomes without isolated free drugs were dissolved in 10% Triton X-100 and PBS. The EE was determined by dividing the amount of drug in the liposome fraction by the amount of drug in total fractions [20].

2.3 Optimization of S-UNL-E formulation

Using the orthogonal experiment analysis, several factors were trialed to achieve optimal formulation, including drug-lipid mass ratio (factor A),

phospholipid-stearamide amount of substance ratio (factor B), cholesterol-phospholipid mass ratio (factor C) and organic-aqueous phases volume ratio (factor D) during the fabrication process. Only one factor was replaced in each series of experiments. Based on the investigation of factors, the four aforementioned factors were selected, and three levels of each factor were designated for the orthogonal design, with the EE as the investigating indicator to screen the formulation. EDTMP with different concentrations were selected as variables when S-UNL-E was prepared.

2.4 Characterization of DAP-FL

The mean particle size, polydispersity index, and zeta potential of the liposome vesicles were determined using laser particle size analyzer dynamic light scattering (Zetasizer Nano ZS, Malvern, Worcestershire, UK) at 25°C. Before characterization, the samples were further diluted with phosphate-buffered solution to form a liposome suspension with a total lipid concentration of 5 mg/mL. Transmission electron microscopy was used to characterize the morphology of the liposome vesicles using a negative staining method. Samples were pretreated with 2% phosphotungstic acid and then air-dried before measurement.

2.5 Primary culture of osteoblasts

Osteoblasts for the primary culture were isolated from calvariae of 1- to 3-day-old Sprague-Dawley (SD) rats. The osteoblasts were cultured in DMEM containing 10% fetal bovine serum, penicillin (100 U/ml), and streptomycin (100 U/mL). All cell cultures were maintained in humidified 5% CO₂ incubators at 37°C. The growth of osteoblasts was observed under an inverted-phase contrast microscope [21].

2.6 Purification and passage of osteoblasts

The culture flask was used for incubation at 37°C in a 5% CO₂ incubator and subculture cells until 80% fusion. The digested cells were cultured at 37°C for 20 min before the non-adherent cells were transferred to another culture flask. The

procedures were repeated twice, and the culture medium was replaced every 2 d.

2.7 Grouping of osteoblasts

S-UNL-E, S-UNL, single scutellarin (S), and blank control (BC) were divided into four groups. S-UNL-E and S-UNL were divided into four groups based on concentrations (2.5×10^6 – 2.5×10^9), including S-UNL-E (2.5×10^6), S-UNL-E (2.5×10^7), S-UNL-E (2.5×10^8), S-UNL-E (2.5×10^9) and S-UNL (2.5×10^6), S-UNL (2.5×10^7), S-UNL (2.5×10^8), and S-UNL (2.5×10^9).

2.8 Morphology of osteoblasts under a microscope

The morphological changes and growth of osteoblasts were observed and photographed under an inverted microscope at a specific time every day.

2.9 Alkaline phosphatase staining

Cells were seeded at 1×10^4 per well in 24-well plates. Staining working liquid was added and incubated at room temperature in the dark for 30 min. Cells with alkaline phosphatase activity were dyed purple-black or blue-black [22].

2.10 Alizarin red S staining

Cells were seeded at 1×10^5 per well in 6-well plates (round wells), fixed with 4% paraformaldehyde for 30 min. Subsequently, 500 μ L alizarin red S staining solution was supplemented to cover the cell surface and incubated at room temperature avoiding light for 20 min. When it was dry, staining results were observed [23].

2.11 Proliferation assay

MTT assays were performed to assess the rate of cell proliferation. Briefly, cells were seeded in 96-well plates at a density of 1×10^4 cells/well and cultured for 5 d. The absorbance at 450 nm was measured in real time every 24 h after incubation by supplementing with 20 μ L of MTT labeling reagent solution (Promega) for 2 h.

2.12 Determination of alkaline phosphatase activities

Cells were seeded at 1×10^4 per well in 24-well plates, washed with PBS and then lysed with a cell lysis buffer (Tris-HCl 25 mM, TritonX-100 0.5%) at 4°C for 2 h. After lysis completion, 100 μ L p-NPP was added to 50 μ L cell lysate and the mixture was incubated at 37°C for 20 min. Meanwhile, 5 μ L cell lysate was added for protein quantification using enhanced BCA protein assay kit (Beyotime, China). The absorbance at 520 nm was detected by a spectrophotometric method. ALP activities were normalized by protein concentrations.

2.13 Determination of bone content

Osteocalcin concentration of osteoblasts were determined by an enzyme-linked immunosorbent assay. Briefly, the sample was balanced for 30 min, samples and enzyme-linked affinity were added to an enzyme-linked plate pore and mixed well at room temperature. Substrates I and II were added to the sample and mixed well, and a termination solution was added and mixed well. The sample was detected by enzyme labeling at 450 nm wavelength [24].

2.14 Determination of fluorescence microscopy

Cells were seeded at 1×10^4 per well in 24-well plates. On the third day, the cells were fixed and closed by 4% paraformaldehyde. The cells were stained using rhodamine – ghost pen cyclic and DAPI after 1 h and observed by a fluorescence microscope.

2.15 Statistical analysis

Data were represented as mean \pm standard deviation. For statistical comparisons, the data were analyzed by one-way analysis of variance (ANOVA) using SPSS (Version 22.0). $p < 0.05$ was considered statistically significant.

3. Results

In this study, we speculated that S-NUL-E could promote bone formation and improve bone mass and bone quality in the implantation area. A reverse

Table 1. Factor levels table of the orthogonal design.

A	B	C	D	E
2:1	5:1	5:1	5:1	10
3:1	10:1	6:1	6:1	20
4:1	15:1	7:1	7:1	30
5:1	20:1	8:1	8:1	40

Note: Phospholipid-cholesterol mass ratio (factor A, mg/mg), phospholipid-scutellarin mass ratio (factor B, mg/mg) phospholipid-sodium cholate mass ratio (factor C, mg/mg), phospholipid-stearamide mass ratio (factor D, mg/mg), EDTMP mass (factor E, mg).

phase evaporation technique was performed to prepare S-UNL-E, and scutellarin encapsulation was subsequently compared. Meanwhile, the optimal preparation option was developed using an orthogonal method, and the particle size was determined using laser light scattering. In osteoblasts cultured in vitro, MTT, ALP staining and alizarin red staining were used to detect the osteogenic effects of S-UNL-E. Our results demonstrated the potential of S-NUL-E in the treatment of poor bone mass and bone quality in the implantation area by its osteogenesis.

3.1 Preparation and optimization of S-UNL-E

When S-UNL-E process was prepared and modified, the mass ratios of phospholipid-cholesterol (factor A), phospholipid-breviscapine (factor B), phospholipid-sodium cholate (factor C), phospholipid-stearamide (factor D) and EDTMP mass (factor E) were taken into consideration. L16 (45) table was referred for orthogonal tests (Table 1), and the optimal preparation process of S-UNL-E was determined. The results are presented in Table 2. The encapsulation was applied as a detection index, and the test number was A1B3C3D3E3 for preparing S-UNL-E as the best process conditions, with mass ratios of phospholipid-cholesterol at 2:1, phospholipid-breviscapine 15:1, phospholipid-sodium cholate 7:1, and phospholipid-stearamide 7:1. The mass of EDTMP was at 30 mg. Under the described conditions, encapsulation was 75.7%.

3.2 Characterization of S-UNL-E

S-UNL-E was prepared according to the best solution A1B3C3D3E3. Liposome particle size and potential were measured by a laser particle size analyzer, and the distribution was uniform and normal. The span should be small (Figure 1).The

Table 2. Results and visual analysis of the orthogonal design experiments.

NO.	A	B	C	D	E	Encapsulation efficiency /%
1	1	1	1	1	1	44.3
2	1	2	2	2	2	64.5
3	1	3	3	3	3	75.7
4	1	4	4	4	4	71.8
5	2	1	2	3	4	63.9
6	2	2	1	4	3	58.2
7	2	3	4	1	2	55.7
8	2	4	3	2	1	48.1
9	3	1	3	4	2	46.2
10	3	2	4	3	1	49.0
11	3	3	1	2	4	42.2
12	3	4	2	1	3	57.3
13	4	1	4	2	3	47.1
14	4	2	3	1	4	53.3
15	4	3	2	4	1	44.9
16	4	4	1	3	2	48.5
Mean1	64.1	50.4	48.3	52.7	46.6	
Mean2	56.5	56.3	57.7	50.5	53.7	
Mean3	48.7	54.6	55.8	59.3	59.6	
Mean4	48.5	56.4	55.9	55.3	57.8	
Range	15.6	6.1	9.4	8.8	13.0	

results showed that average particle size of S-UNL-E was 156.67 ± 1.76 nm, and Zeta potential was -28.77 ± 0.66 mV (Table 3). It indicated the presence of great electrostatic repulsive force between S-UNL-E particles with satisfactory stability.

3.3 S-UNL-E regulates the proliferation of osteoblasts

Subsequently, to clarify the regulatory function of S-UNL-E on osteoblasts, we added different concentrations of S-UNL-E to rat skull osteoblasts cultured in vitro. The osteoblasts were observed under a microscope. After 24 h culture, the cells adhered to the wall and presented triangular or spindle-shape and cell protrusion (Figure 2a). The isolated osteoblasts were identified by ALP staining and calcium nodular staining. Microscopically, ALP active site was dark blue or blue-purple, and the nucleus was red (Figure 2b). This calcium nodule staining exhibited that osteoblasts were stained as orange-red calcium nodules (Figure 2c). All these findings indicated that isolated osteoblasts exerted a role of osteogenic function. MTT assays showed that the cells grew slowly on the first and second days. From the third to the fifth day, they grew rapidly and stayed in the logarithmic growth stage, reached the maximum on the 5th day, and then grew slowly and entered

the plateau stage (Figure 2d). S-UNL-E and S-UNL at concentrations of 2.5×10^6 , 2.5×10^7 , 2.5×10^8 , 2.5×10^9 were added, respectively, to compare the functional differences. MTT assay results showed that S-UNL-E could improve the OD value of MTT assay (Figure 3a-3d), indicating that S-UNL-E promoted the proliferation of osteoblasts. Compared with the four concentrations, S-UNL-E (2.5×10^8) had the best effect on proliferation (Figure 3e-3f)

3.4 S-UNL-E promotes osteoblast differentiation

To clarify S-UNL-E effect on the differentiation of osteoblasts, ALP staining showed that the osteoblasts of S-UNL-E stained more deeply, and the ALP activity assay showed that S-UNL-E significantly increased the expression of ALP in osteoblasts (Figure 4a-4b). Following comparison of the four concentrations, S-UNL-E (2.5×10^8) produced the best effect in differentiation promotion, and at the same concentration, S-UNL-E had better osteogenic differentiation than the S-UNL group (figure 4f). The same results were revealed in detecting mineralized nodules and osteocalcin protein content, indicating S-UNL-E markedly increased osteoblast differentiation (Figure 5). Following comparison of the four concentrations, S-UNL-E (2.5×10^8) produced the best effect in

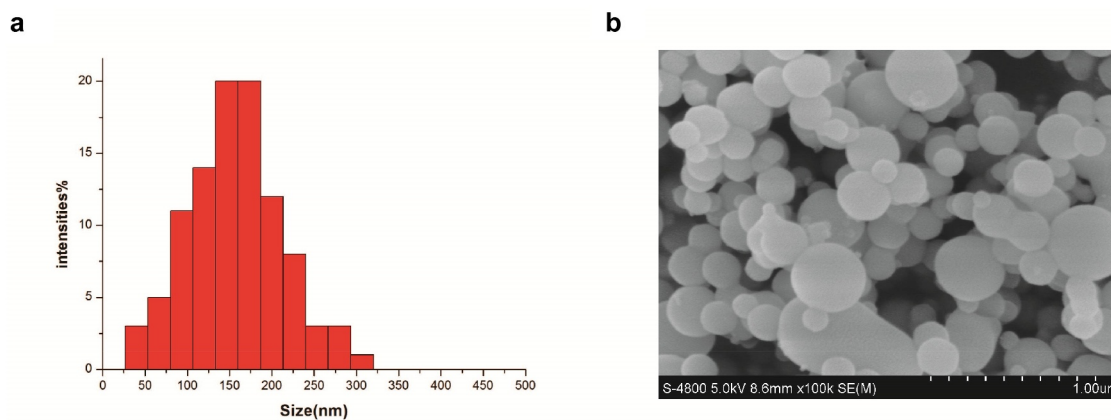


Figure 1. S-UNL-E particle size analysis and morphologic observation. (a) Results of particle size analysis. (b) S-UNL-E particle observation by transmission electron microscopy.

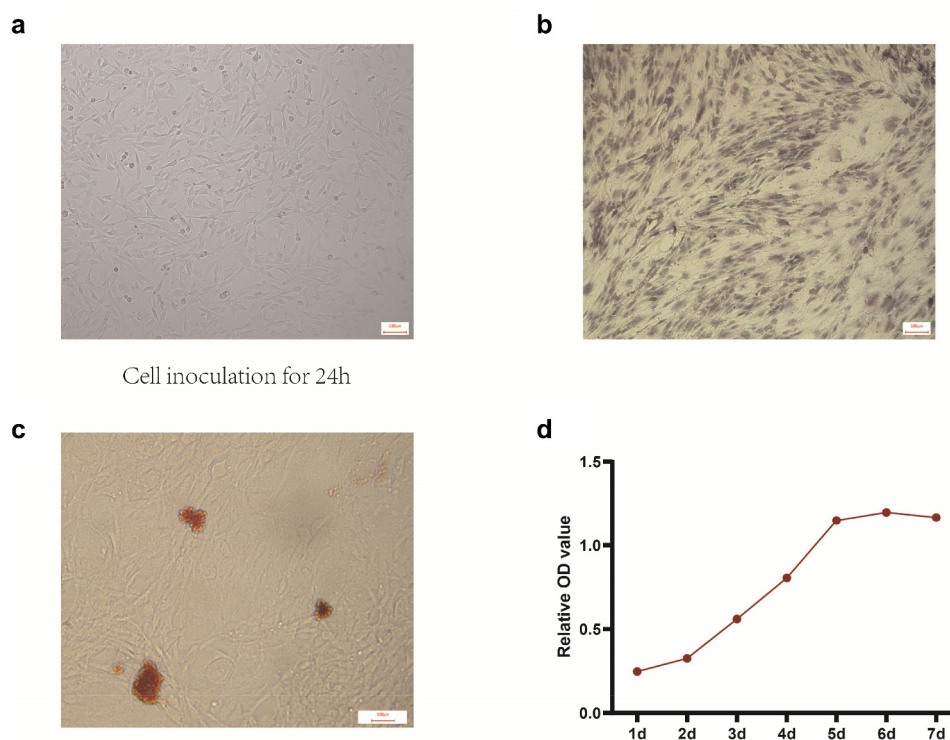


Figure 2. Isolation and culture of osteoblasts. (a) Osteoblast morphology observed under white light. (b) Identification of osteoblast differentiation using ALP staining. (c) Determination of osteogenic differentiation by alizarin red staining. (d) Determination of cell proliferation activity by MTT. Scale bar: 100 μ m.

differentiation promotion, and at the same concentration, S-UNL-E had better osteogenic differentiation than the S-UNL group (figure 5f). Calcified nodules in each group were visualized using scanning electron microscopy, and it was clearly displayed that the S-UNL-E (2.5×10^8) group presented the largest number of calcified nodules (Figure 6a). The results of cytoskeletal

actin staining revealed that the cells in the S-UNL-E group were densely distributed with integrated cell structure, and the actin filaments were clear and obvious (Figure 6b). The previously described results revealed that S-UNL-E greatly promoted the differentiation and maturation of osteoblasts, and S-UNL-E (2.5×10^8) produced the most favorable effect in differentiation

Table 3. S-UNL-E particle size analysis and Zeta potential detection.

	Size (nm)	Zeta potential (mv)
1	158.5	-29.7
2	154.3	-28.2
3	157.2	-28.4
$\bar{x} \pm s$	156.67 ± 1.76	-28.77 ± 0.66

bone tissue engineering. Finding a simple, cheap, safe and inducing endogenous bone tissue growth to promote bone regeneration is a current research hotspot and challenge. The present study constructed a sustained-release system of scutellarin loaded with bone target flexible nanoliposomes

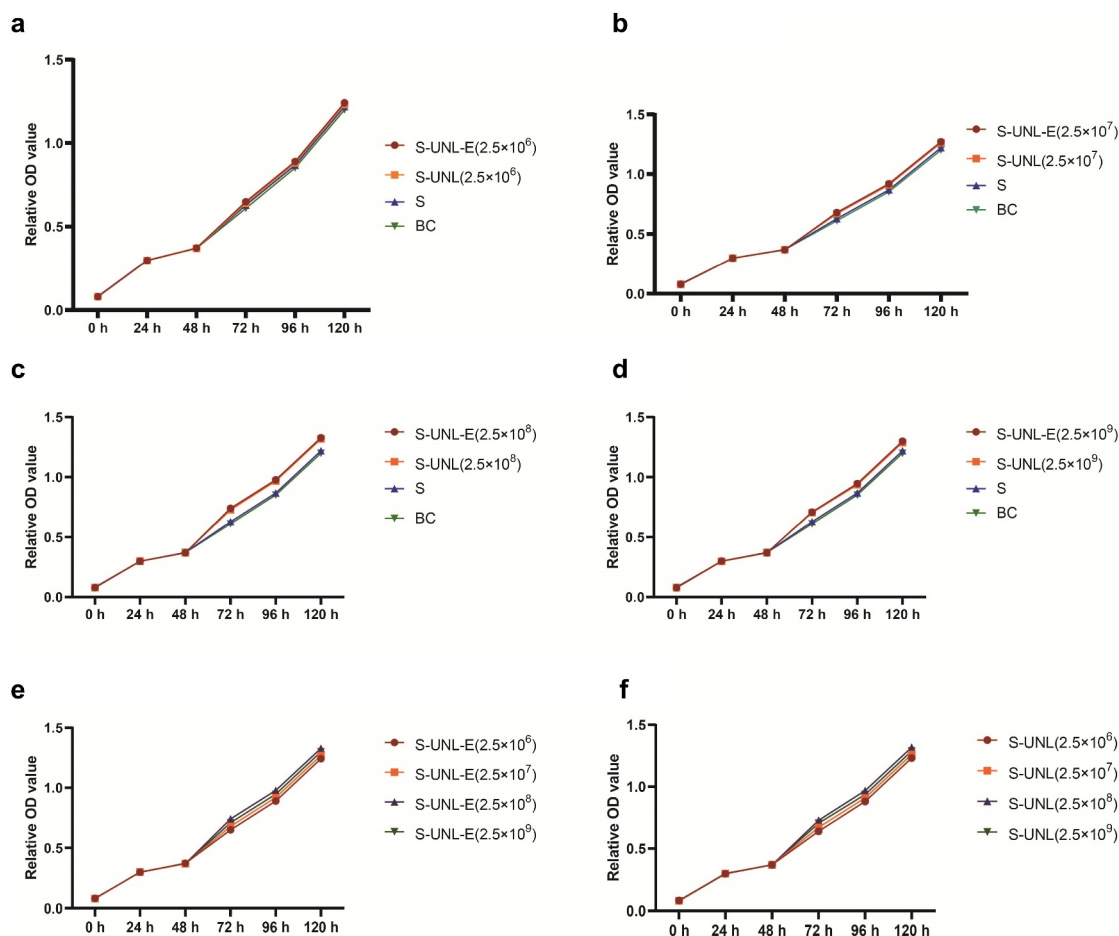


Figure 3. Determination of S-UNL-E regulation on the proliferation of osteoblasts by MTT. MTT assay was used to detect the effect of S-UNL-E on the proliferation of osteoblasts, and the proliferation curve was plotted based on the number of osteoblasts at the five time points of 24 h, 48 h, 72 h, 96 h and 120 h. (a-d) OD values treated at concentrations of 2.5×10^6 , 2.5×10^7 , 2.5×10^8 , and 2.5×10^9 . (e) Regulation of osteoblast proliferation by different concentrations of S-UNL-E. (f) Differential regulation of S-UNL-E and S-UNL on osteoblast proliferation.

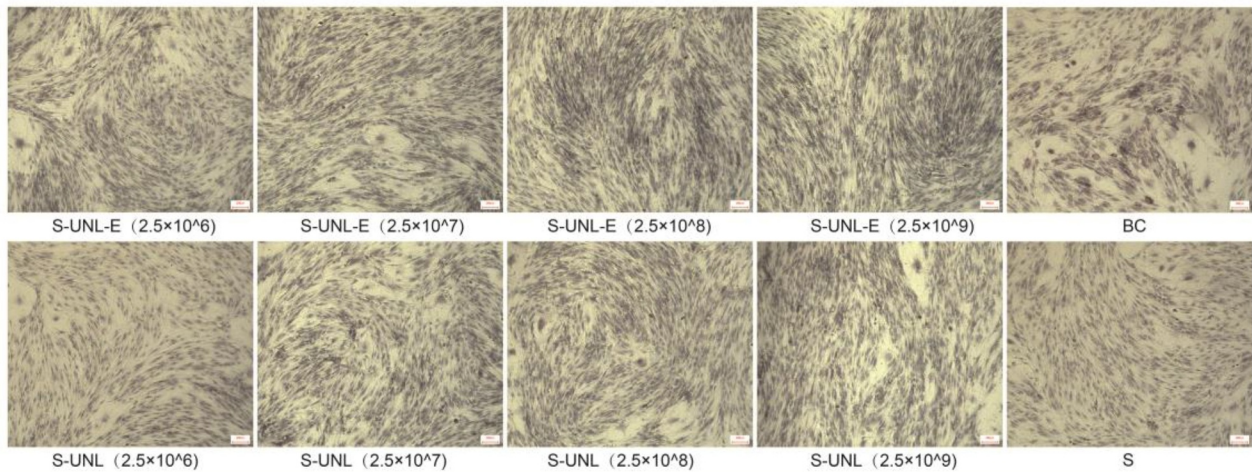
promotion. In addition, compared with the S-UNL group, the effect of the S-UNL-E group was significantly better than that of the S-UNL group.

4 Discussion

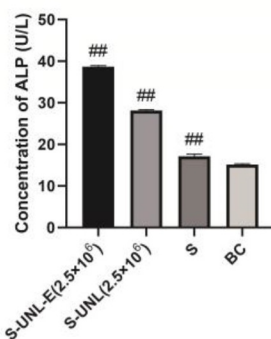
New bone formation around implants is of vital significance in the application and research of

and investigated its regulatory function of in osteoblasts cultured in vitro. The results indicated that the optimal process conditions for S-UNL-E included phospholipid-cholesterol mass ratio of 2:1, phospholipid-breviscapine mass ratio of 15:1, phospholipid-sodium cholate mass ratio of 7:1, and phospholipid-stearamide mass ratio of 7:1, and the mass of EDTMP was 30 mg. In vitro test

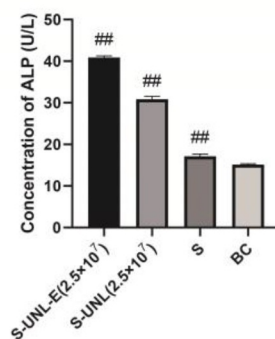
a



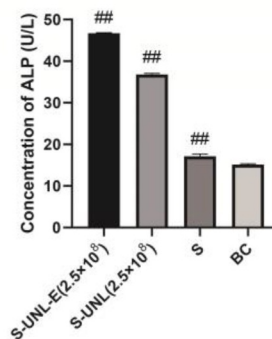
b



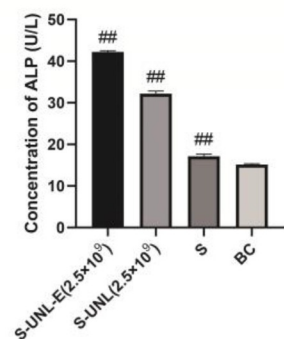
c



d



e



f

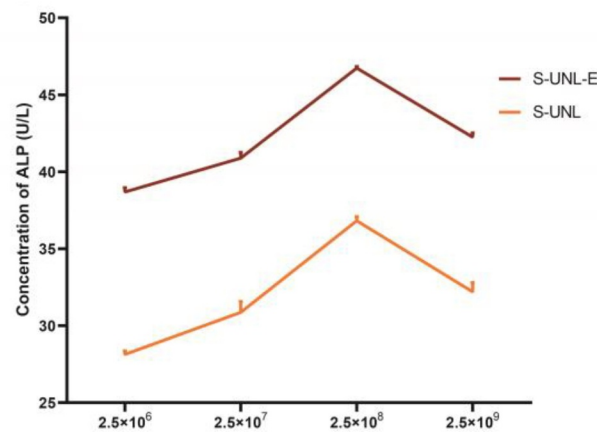


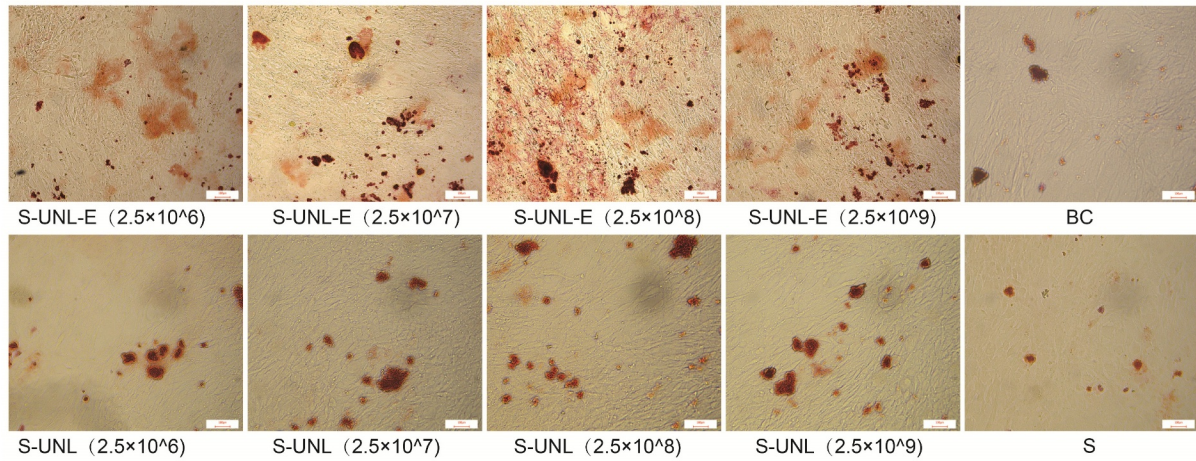
Figure 4. The effect detection of S-UNL-E on osteoblast differentiation by ALP staining. (a) ALP staining result photographs. (b-e) ALP content determination, ALP content treated at concentrations of 2.5×10^6 , 2.5×10^7 , 2.5×10^8 , and 2.5×10^9 . F, The regulation comparison of ALP content in osteoblasts between S-UNL-E and S-UNL. Scale bar: 100 μm . ## $p < 0.01$, compared with BC group.

results showed that S-UNL-E could effectively promote osteogenic differentiation and bone formation. Furthermore, this work offered a novel insight and proposal for solving the problems of

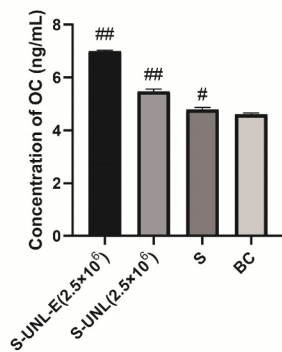
insufficient bone mass and poor bone quality in clinical implantation area.

Scutellarin plays a role in microvascular dilation, reducing blood viscosity, increasing cerebral blood

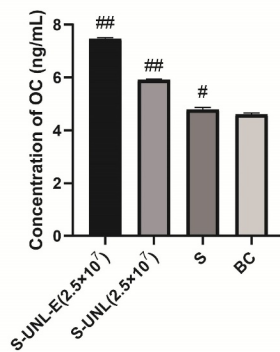
a



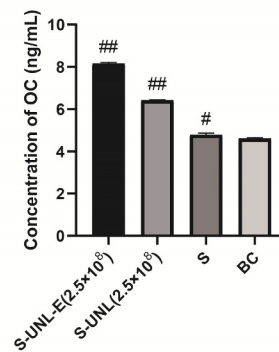
b



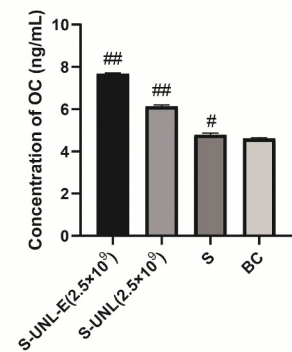
c



d



e



f

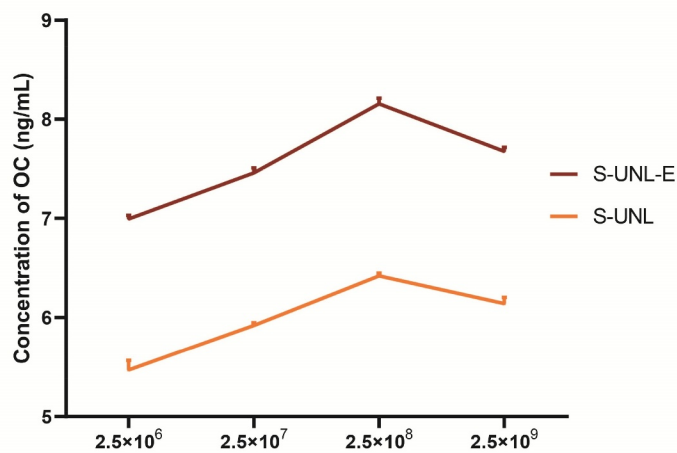


Figure 5. Alizarin red staining and osteocalcin content determination. (a) Alizarin red staining. (b-e) ALP content determination, results of osteocalcin content determination treated at concentrations of 2.5×10^6 , 2.5×10^7 , 2.5×10^8 , and 2.5×10^9 . (f) Regulation of osteocalcin content in osteoblasts between S-UNL-E and S-UNL. Scale bar: 100 μm . ## $p < 0.01$, compared with BC group.

flow, promoting microcirculation, and improving lipid metabolism. It also produces anti-inflammatory, anti-apoptotic, anti-oxidation, and anti-allergic

functions. At present, it is mainly applied to treat cerebrovascular diseases. Scutellarin can induce angiogenesis in vitro, upregulate the expression of

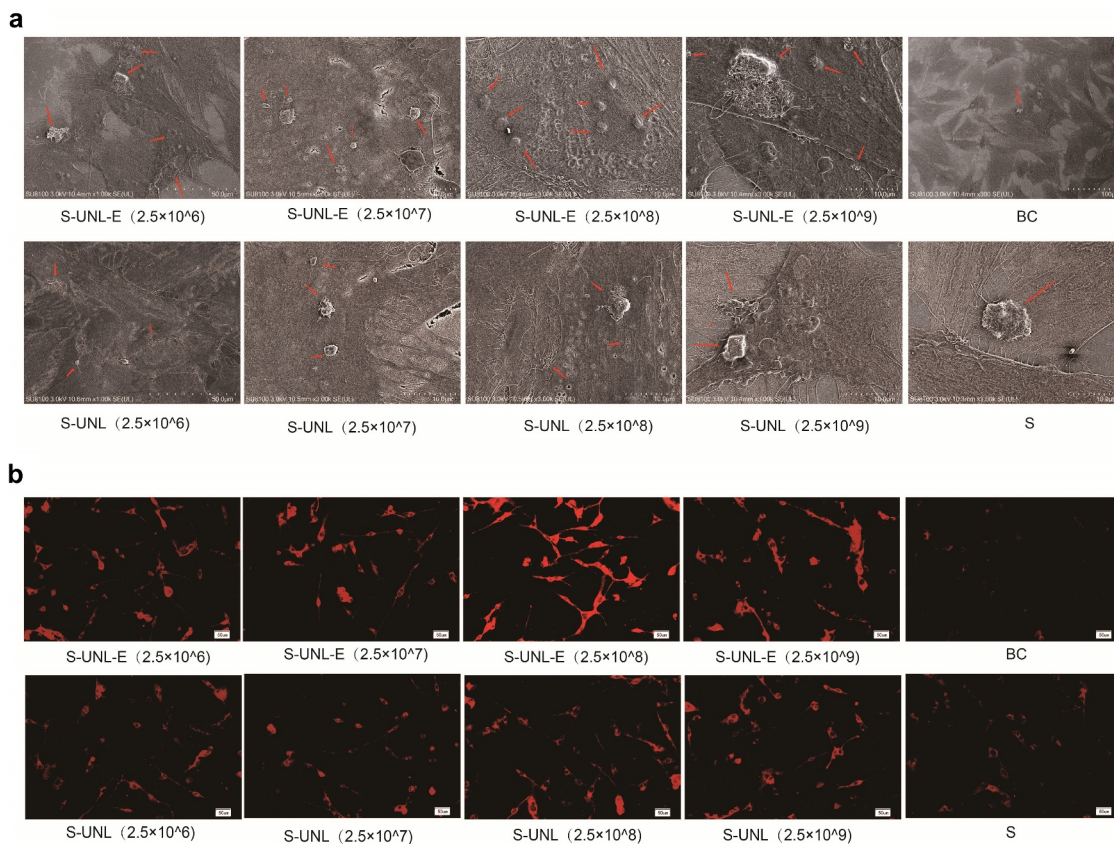


Figure 6. Calcium nodules and actin detection. (a) Calcified nodules in each group were observed by scanning electron microscopy. (b) Cytoskeleton actin staining was observed by fluorescence microscopy. Scale bar: 50 μ m.

the angiogenesis marker PECAM-1, and significantly increase the mRNA content and activity of the angiogenesis-related factor MMP-2. It is therefore that this agent can be used as a potential angiogenesis inducer to treat ischemic diseases and promote wound healing [25,26]. Recent studies have reported that scutellarin can regulate bone metabolism. It can upregulate BMP2 transcriptional activity and mRNA expression levels, induce osteogenic differentiation by activating the BMP pathway, and inhibit osteoclast differentiation through negative regulation of RANKL-mediated MAPKs and NF- κ B signaling pathways. As a result, osteoporosis can be treated, and osteolysis caused by sustained release of titanium particles can be prevented in joint prosthesis [27,28]. In this work, we divided four groups: the bone formation of osteoblasts was increased in the S-UNL-E group, S-UNL group, and S group after treatment, which was higher than that of the control group. This was consistent with

the results of previous studies showing that baicalin induces osteogenic differentiation.

In the current targeting guide and vector system, liposomes gain popularity due to easy preparation, nontoxicity, non-immunogenicity, easy carrying and release of various drugs, as well as delivery of the target drug to a specific site by modification. Using microvesicles formed by liposomes, the drug is encapsulated in a layered phase-controlled lipid bilayer, which has strong permeability and is easily taken up by phagocytes to achieve intracellular drug delivery, which improves the bioavailability of the drug and reduces dosage thereby minimizing or even avoiding adverse reactions of drugs. In the prevention and treatment of dental caries and periodontal disease, drug delivery by liposome can inhibit bacteria and reduce inflammation. Meanwhile, calcium, phosphorus and other minerals can be induced to precipitate on the surface of hard tissue

to promote mineralization [29]. The new flexible nanoliposome has good deformability, allowing more particles to pass through the bone marrow-blood barrier. Hydroxyapatite in the bone matrix was adopted as an action target, a flexible nanoliposome with both active and passive bone targeting effects was designed and prepared, and its properties were preliminarily studied. Compared with unmodified flexible nanoliposomes, the peak drug concentration in the bone reached 3.81 times of the original peak concentration, and the total targeting efficiency was increased by 653.02% [30]. In this study, we prepared EDTMP-modified flexible nanoliposomes and its encapsulation reached up to 80%. The current study adopted the optimal preparation process of S-UNL-E selected by orthogonal experiments to prepare and optimize S-UNL-E process, and the obtained encapsulation of S-UNL-E was 75.7%. The findings demonstrated that S-UNL-E greatly promoted the differentiation and maturation of osteoblasts, and S-UNL-E (2.5×10^8) produced the most favorable effect in differentiation promotion. Compared with previous studies, this study had better encapsulation and electrostatic stability, and it presented a satisfactory function in promoting bone formation in experimental verification.

5. Conclusions

The present study successfully constructed an S-UNL-E material characterized by high encapsulation and high stability. The optimal process conditions for S-UNL-E included phospholipid-cholesterol mass ratio of 2:1, phospholipid-breviscapine mass ratio of 15:1, phospholipid-sodium cholate mass ratio of 7:1, and phospholipid-stearamide mass ratio of 7:1, and the mass of EDTMP was 30 mg. S-UNL-E greatly promoted the differentiation and maturation of osteoblasts, and S-UNL-E (2.5×10^8) produced the most favorable effect in differentiation promotion. This work offered a research foundation for solving the problems of insufficient bone mass and poor bone quality of implantation areas in clinic. In future research, we will further explore S-UNL-E's targets and molecular regulation mechanisms, and study its therapeutic effects in animal models.

Highlights

- S-UNL-E was obtained using a reverse phase evaporation technique.
- S-UNL-E promoted osteogenic differentiation and bone formation.
- S-UNL-E (2.5×10^8) produced the most favorable effect in promoting bone formation.

Disclosure statement

No potential conflict of interest was reported by the author(s).

Funding

This study was supported by the National Natural Science Foundation of China Youth Science Fund Project (81800940) and Qingdao Postdoctoral Researcher Applied Research Project.

References

- [1] Garcia-Gonzalez M, Blason-Gonzalez S, Garcia-Garcia I, et al. Optimized planning and evaluation of dental implant fatigue testing: a specific software application. *Biology (Basel)*. 2020;9(11): 372.
- [2] Xie Y, Li S, Zhang T, et al. Titanium mesh for bone augmentation in oral implantology: current application and progress. *Int J Oral Sci*. 2020;12(1):37.
- [3] Liu F, Li L, Lu W, et al. Scutellarin ameliorates cartilage degeneration in osteoarthritis by inhibiting the Wnt/beta-catenin and MAPK signaling pathways. *Int Immunopharmacol*. 2020;78:105954.
- [4] Xiong LL, Du RL, Xue LL, et al. Anti-colorectal cancer effects of scutellarin revealed by genomic and proteomic analysis. *Chin Med*. 2020;15:28.
- [5] Xu LJ, Chen RC, Ma XY, et al. Scutellarin protects against myocardial ischemia-reperfusion injury by suppressing NLRP3 inflammasome activation. *Phytomedicine*. 2020;68:153169.
- [6] Peng L, Wen L, Shi QF, et al. Scutellarin ameliorates pulmonary fibrosis through inhibiting NF-kappaB/NLRP3-mediated epithelial-mesenchymal transition and inflammation. *Cell Death Dis*. 2020;11(11):978.
- [7] Wang J, Zhao B, Yang S, et al. Scutellarin enhances osteoblast proliferation and function via NF-kappaB-mediated CXCR4 induction. *Gene*. 2018;676:29–36.
- [8] Zhao S, Sun Y, Li X, et al. Scutellarin inhibits RANKL-mediated osteoclastogenesis and titanium particle-induced osteolysis via suppression of

- NF-kappaB and MAPK signaling pathway. *Int Immunopharmacol.* **2016**;40:458–465.
- [9] Zhao Z, Chen C, Xie C, et al. Design, synthesis and evaluation of liposomes modified with dendritic aspartic acid for bone-specific targeting. *Chem Phys Lipids.* **2020**;226:104832.
- [10] Li C, Zhang X, Huang X, et al. Preparation and characterization of flexible nanoliposomes loaded with daptomycin, a novel antibiotic, for topical skin therapy. *Int J Nanomedicine.* **2013**;8:1285–1292.
- [11] El SS. Enhancing anticancer effects, decreasing risks and solving practical problems facing 3-bromopyruvate in clinical oncology: 10 years of research experience. *Int J Nanomedicine.* **2018**;13:4699–4709.
- [12] Munawaroh HSH, Gumilar GG, Nurjanah F, et al. In-vitro molecular docking analysis of microalgae extracted phycocyanin as an anti-diabetic candidate. *Biochem Eng J.* **2020**;161(15):107666–107682.
- [13] Low SS, Chen Z, Li Y, et al. Design principle in biosensing: Critical analysis based on graphitic carbon nitride (G-C3N4) photoelectrochemical biosensor. *Trends Analyt Chem.* **2021**;145(1):116454–116464.
- [14] Nielsen JJ, Low SA. Bone-Targeting systems to systemically deliver therapeutics to bone fractures for accelerated healing. *Curr Osteoporos Rep.* **2020**;18(5):449–459.
- [15] Song H, Li X, Zhao Z, et al. Reversal of osteoporotic activity by endothelial cell-secreted bone targeting and biocompatible exosomes. *Nano Lett.* **2019**;19(5):3040–3048.
- [16] Choi JY. Treatment of bone metastasis with bone-targeting radiopharmaceuticals. *Nucl Med Mol Imaging.* **2018**;52(3):200–207.
- [17] Lange R, Ter Heine R, Knapp RF, et al. Pharmaceutical and clinical development of phosphonate-based radiopharmaceuticals for the targeted treatment of bone metastases. *Bone.* **2016**;91:159–179.
- [18] Pandit-Taskar N, Larson SM, Carrasquillo JA. Bone-seeking radiopharmaceuticals for treatment of osseous metastases, Part I: alpha therapy with ²²³Ra-dichloride. *J Nucl Med.* **2014**;55(2):268–274.
- [19] Ashrafzadeh MS, Akbarzadeh A, Heydarinasab A, et al. In vivo glioblastoma therapy using targeted liposomal cisplatin. *Int J Nanomedicine.* **2020**;15:7035–7049.
- [20] Li W, Zhou M, Xu N, et al. Comparative analysis of protective effects of curcumin, curcumin-beta-cyclodextrin nanoparticle and nanoliposomal curcumin on unsymmetrical dimethyl hydrazine poisoning in mice. *Bioengineered.* **2016**;7(5):334–341.
- [21] Liao F, Hu X, Chen R. The effects of Omarigliptin on promoting osteoblastic differentiation. *Bioengineered.* **2021**. doi:10.1080/21655979.2021.1999366.
- [22] Lei X, Liu Q, Li S, et al. Effects of fluid shear stress on expression of focal adhesion kinase in MG-63 human osteoblast-like cells on different surface modification of titanium. *Bioengineered.* **2021**;12(1):4962–4971.
- [23] Peng Z, Lu S, Lou Z, et al. Exosomes from bone marrow mesenchymal stem cells promoted osteogenic differentiation by delivering miR-196a that targeted Dickkopf-1 to activate Wnt/beta-catenin pathway. *Bioengineered.* **2021**. doi:10.1080/21655979.2021.1996015.
- [24] Chai Y, Pu X, Wu Y, et al. Inhibitory effect of *Astragalus Membranaceus* on osteoporosis in SAMP6 mice by regulating vitaminD/FGF23/Klotho signaling pathway. *Bioengineered.* **2021**;12(1):4464–4474.
- [25] Zhou QB, Jin YL, Jia Q, et al. Baicalin attenuates brain edema in a rat model of intracerebral hemorrhage. *Inflammation.* **2014**;37(1):107–115.
- [26] Shin JW, Kang HC, Shim J, et al. *Scutellaria baicalensis* attenuates blood-brain barrier disruption after intracerebral hemorrhage in rats. *Am J Chin Med.* **2012**;40(1):85–96.
- [27] Lee SI, Kim SY, Park KR, et al. Baicalein promotes angiogenesis and odontoblastic differentiation via the BMP and Wnt pathways in human dental pulp cells. *Am J Chin Med.* **2016**;44(7):1457–1472.
- [28] Liao H, Ye J, Gao L, et al. The main bioactive compounds of *Scutellaria baicalensis* Georgi. for alleviation of inflammatory cytokines: a comprehensive review. *Biomed Pharmacother.* **2021**;133:110917.
- [29] Chen H, Gu L, Liao B, et al. Advances of anti-caries nanomaterials. *Molecules.* **2020**;25(21): 5047.
- [30] Guo J, Zhang M, Li YF, et al. [Bone-targeted ultradeformable nanoliposomes]. *Beijing Da Xue Xue Bao Yi Xue Ban.* **2009**;41(2):203–207.